

## HIGH RESOLUTION SIMULATION OF FILM COOLING WITH BLOWING RATIO AND INCLINATION ANGLE EFFECTS BASED ON HYBRID THERMAL LATTICE BOLTZMANN METHOD

by

**Yanqin SHANGGUAN<sup>a,b,c\*</sup>, Xian WANG<sup>b</sup>,  
Fei CAO<sup>a</sup>, and Yandan ZHU<sup>d</sup>**

<sup>a</sup>College of Mechanical and Electrical Engineering,  
Hohai University, Nanjing, Jiangsu, China

<sup>b</sup>State Key Laboratory for Strength and Vibration of Mechanical Structures,  
Xi'an Jiaotong Xi'an, Shaanxi, China

<sup>c</sup>Key Laboratory of Icing and Anti/De-Icing,  
China Aerodynamics Research and Development Center, Mianyang, Sichuan, China

<sup>d</sup>Computational Aerodynamics Institute,  
China Aerodynamics Research and Development Center, Mianyang, Sichuan, China

Original scientific paper

<https://doi.org/10.2298/TSCI210424286S>

*A series of high resolution simulations on film cooling with varying blowing ratios and inclination angles are carried out by using in-house code based on hybrid thermal lattice Boltzmann method. Three blowing ratios ranging from 0.2-0.8 and four inclination angles from 15° to 60° are chosen for the simulations. The evolutionary mechanism of coherent structure in three domains of film-covering region is studied from the view of space and time. Besides, the influencing mechanism of blowing ratio and inclination angle on flow and heat transfer features of film cooling is uncovered. Results show that hairpin vortex, hairpin packet, and quasi-streamwise vortex appearing in rotating domain play a key role in heat transfer process of film cooling. The strong ejection, sweep and vortex rotation resulted from these vortices enhance the convective heat transfer. It is also found that the size of coherent structure varies significantly with blowing ratio and its integral form shows a strong dependence on inclination angle. Moreover, inclination angle of coolant jet has a significant impact on turbulence fluctuation intensity. The influence of blowing ratio on the attachment of coolant film and film-cooling performance is more obvious than that of inclination angle. It is believed that all of these are related closely to the variation of streamwise and wall-normal jet velocity in the case of various blowing ratios and inclination angles.*

Key words: *hybrid thermal lattice Boltzmann method, evolutionary mechanism, film cooling, blowing ratio, inclination angle, coherent structure, influencing mechanism*

### Introduction

With the daily increasing demand on thermal efficiency and power output of gas turbine, the gas temperature at turbine inlet becomes extremely high. Consequently, cooling of gas turbine components is inevitable. Except for applying thermal barrier coating on blade surface,

\* Corresponding author, e-mail: shanguanyanqin@hhu.edu.cn

cooling system with high efficiency is another essential way to decrease the temperature of blade surface, in which film cooling is one of the most important cooling methods [1] and studied by extensive researchers.

The main principle of film cooling is that a stream of coolant gas is injected from a hole drilled on the wall along tangent direction or at a certain inclination angle to form a thin coolant-film layer, protecting the surface from direct exposure to the cross-flow with high temperature. Simulation and experiment are the ways to study film cooling. Han *et al.* [2] made a detailed explanation on film cooling and presented plenty of experiment results. Acharya [3] made a comprehensive review on lots of numerical works of film cooling during recent twenty years. No matter experimental or numerical works, most of them are concerned about the effects of various aerodynamic and geometrical parameters, such as blowing ratio (BR), inclination angle, the shape of film cooling hole and compound angle on cooling performance [4-8]. However, there seems few studies on the influencing mechanism of these parameters and the evolutionary mechanism of coherent structure, which are pivotal and theoretical problems for film-cooling investigation. If the evolutionary process of coherent structure can be clearly understood, also how to adjust the parameters to form a stable and efficient coolant film layer, simple configurations of film cooling hole with good cooling performance may be proposed. Thus, the manufacturing costs of blade would be dramatically reduced. The mixing between jet and cross-flow arises large amount of coherent structures. Investigation on film cooling from the coherent structure perspective is necessary. For the numerical simulation, it is need to obtain the instantaneous coherent structures with various scales and their interactions accurately. It is a great challenge for computational scheme and tool to capture the instantaneous flow dynamics in turbulence simulation.

Nowadays, most of the turbulence simulations of film cooling are based on time-averaged method, Reynolds averaged Navier-Stokes equation (RANS), however, it has some shortages. For example, Lakehal *et al.* [9] calculated temperature and velocity fields with various BR and concluded that the secondary-flow and heat transfer mechanisms occurring in viscosity-affected near-wall layer are difficult to be predicted precisely by  $k-\varepsilon$  based on two-layer turbulence model. After a few years, Theodoridis *et al.* [10] conducted 3-D calculations of the flow field around a turbine blade with film cooling injection near leading edge. It was found that the lateral jet spreading on pressure side was under-predicted by the standard  $k-\varepsilon$  turbulence model with wall functions. Dyson *et al.* [11] adopted a modified model,  $k-\varepsilon$  SST turbulent model, to study performance of film cooling. The results showed that the  $k-\varepsilon$  SST RANS model over-predicted local adiabatic film effectiveness and overall cooling effectiveness for an attached jet, while performance was under-predicted for a detached jet. Galeazzo *et al.* [12] made the simulations on turbulent mixing in a jet in cross-flow respectively by RANS and large eddy simulation (LES). The numerical results indicated that LES can accurately capture large-scale coherent structure which dominates the turbulent mixing. With the development of computer technology, LES on film cooling becomes prevailing. Renze *et al.* [13] investigate the effect of density gradient on flow characteristics of film cooling by using LES. Shangguan *et al.* [14] conducted a numerical simulation based on LES to study the flow characteristics of film cooling. Recently, LES was performed by Qenawy *et al.* [15] to analyze unsteady flow behaviors of a flat plate film cooling. Andrew *et al.* [16] performed a blind LES of film cooling with a canonical cylindrical cooling hole geometry using a massively-parallel solver and obtained accurate results. It took about two months to accomplish the simulation with about 88.7 million meshes. In order to capture the detailed unsteady behaviors of coherent structure, higher solution computational mesh is indispensable. However, heavy computation load and long-time consumption are still the bottleneck for LES.

In the last few years, the application of graphic processing unit (GPU) on CFD provides hope to researchers devoting to turbulence study. The GPU has become prevailing for general purpose because of its high performance of floating-point arithmetic operation, wide memory bandwidth, and good programmability [17]. On the other hand, lattice Boltzmann method (LBM), one of the meso-scale methods, shows a fast development and has been regarded as a promising alternative for flow simulation. It is mainly because that LBM has the advantages of easy implementation of boundary conditions, simple programming, and fully parallel algorithms [18]. Significantly, the fully parallel algorithm of LBM makes it match perfectly with GPU [19], which greatly improves the computational efficiency. Therefore, the high resolution simulation based on LBM-GPU has the considerable potential to fulfill detailed turbulence investigation.

In order to capture fine coherent structure and obtain adequate fine quantitative results, this work attempt to reproduce this complicated mixing process with high resolution simulation by using hybrid thermal lattice Boltzmann method (HTLBM) and multiple graphic processing units (multi-GPU). The standard Smagorinsky subgrid-scale stress (SGS) model of LES is adopted. The simulations are fulfilled in a parallel way on 15 NVIDIA Telsa K20M GPU. Based on the three-domain definition of film-covering region proposed in our previous work [20], the spatially and temporally evolutionary mechanisms of coherent structure in each domain is studied in detail and the influencing mechanism of BR and inclination angle on flow behavior and cooling performance is uncovered to deepen the understanding of mixing mechanism of film cooling.

## Computational details

### Computational domain and boundary conditions

Figure 1 shows the geometry of film cooling computational domain. Film cooling hole with the length of  $l = 3D$  inclined at a certain angle is drilled on the bottom wall. The surface of the bottom wall is extended  $10D$  in the upstream direction of the center of film cooling hole. The computational domain is extended till  $25D$  in the downstream of the center of film cooling hole,  $3D$  in  $y$ -direction and  $10D$  in  $z$ -direction. Here,  $D$  is the hole diameter. Hot cross-flow enters into computational domain through the inlet with a  $1/7$  power law velocity boundary condition and leaves at the outlet with zero pressure gradient boundary condition. No-slip adiabatic boundary condition is given at the bottom wall surface. Symmetry boundary condition is provided at the top surface. Periodic boundary condition is applied in spanwise direction.

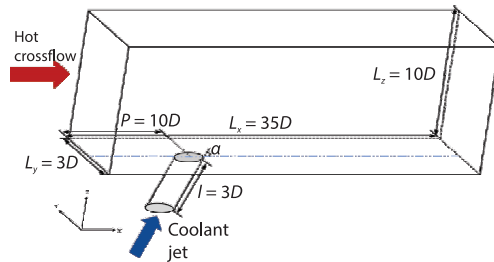


Figure 1. Flow configuration for film cooling

In the simulation of present work, the Reynolds number based on cross-flow velocity  $u_\infty$  and hole diameter  $D$  is set as  $Re = 1000$ . Three BR of 0.2, 0.5, and 0.8 are taken into consideration. Besides, four values of jet inclination angle,  $\alpha$ , are chosen:  $15^\circ$ ,  $30^\circ$ ,  $45^\circ$ , and  $60^\circ$ . The density ratio of coolant jet to hot cross-flow is kept at 1 to neglect the impact of density ratio. Since present work mainly focuses on the effect of BR and inclination angle. The temperature of hot cross-flow,  $T_\infty$ , and the temperature of coolant jet,  $T_j$ , are set as 300 K and 150 K, respectively. The cooling performance is evaluated by non-dimensional temperature  $\theta = (T_{aw} - T_j)/(T_\infty - T_j)$  and adiabatic film cooling effectiveness  $\eta = (T_\infty - T_{aw})/(T_\infty - T_j)$ . Here,  $T_{aw}$  is the temperature of the adiabatic bottom wall. On the other hand, 54 grid points are arranged for the length of

1D, resulting in the total mesh number is  $1.90 \cdot 10^8$ . The uniform grid is arranged in the whole computational domain, causing the mesh near the bottom wall satisfies to  $y^+ < 1$ . Meanwhile, the grid-convergence study has been performed in our previous work [20, 21].

### Solution algorithm

The HTLBM coupled with SGS model is adopted to conduct the simulation on film cooling in this work. The HTLBM is the extension of LBM that couple athermal-lattice Boltzmann equation scheme for flow field and diffusion-advection equation for temperature field explicitly. The grid is generated by discretization of space with uniform length,  $\Delta x$ , and discretization of time with step length,  $\Delta t$ . Time step  $\Delta t$  and lattice spacing  $\Delta x$  are chosen according to lattice units, such that  $\Delta t = 1$  and  $\Delta x = 1$ . Quantities can easily be converted between lattice units and physical units by conversion factors [22].

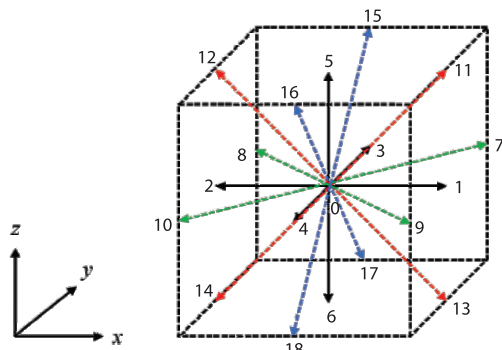


Figure 2. The schematic representation of D3Q19 discrete velocity set

### Lattice Boltzmann equation for flow field

For LBM-based simulation on flow field, a discrete particle density distribution function  $f_i(\vec{x}, t)$  is used to trace the evolution of fluid. The distribution function represents the density of particles with discrete velocity  $\vec{e}_i = (e_{ix}, e_{iy}, e_{iz})$  at position  $\vec{X} = (x, y, z)$  and time  $t$ . The velocity set D3Q19 is adopted for the simulation on fluid-flow. This velocity set is one of the popular choices for 3-D simulation based on LBM. Figure 2 illustrates the schematic representation of D3Q19 discrete velocity set. Note that the speed of sound in lattice unit is  $c_s = 3^{1/2}$  for D3Q19 discrete velocity set.

Multiple-relaxation-time lattice Boltzmann scheme is used to improve the robustness of numerical computation. Referring to [23], the time evolution equation of velocity distribution function,  $\vec{f}$ , can be written:

$$\vec{f}(\vec{X} + [\mathbf{e}]\Delta t, t + \Delta t) - \vec{f}(\vec{X}, t) = -[\mathbf{M}][\mathbf{S}](\vec{m} - \vec{m}^{\text{eq}}) \quad (1)$$

where  $[\mathbf{M}]$  is a  $19 \times 19$  matrix which linearly transforms the distribution function  $\vec{f}$  to the velocity moment  $\vec{m}$ . Their relationship is shown:

$$\vec{m} = [\mathbf{M}]\vec{f} \quad (2)$$

As for the D3Q19 discrete velocity set applied in this work, the equilibrium of the moments  $\vec{m}^{\text{eq}}$  are calculated according to [24]. The relaxation matrix  $[\mathbf{S}]$  is diagonal:

$$[\mathbf{S}] = \text{diag}(0, s_1, s_2, 0, s_4, 0, s_4, 0, s_4, s_9, s_2, s_9, s_2, s_9, s_9, s_9, s_9, s_{16}, s_{16}, s_{16}) \quad (3)$$

To optimize the linear stability of D3Q19 discrete velocity set, the values of the relaxation rates are chosen as:  $s_1 = 1.19$ ,  $s_2 = s_{10} = 1.40$ ,  $s_4 = 1.20$ , and  $s_{16} = 1.98$  [24]. Moreover, the relaxation parameter  $s_9$  is related to the kinematic viscosity,  $\nu$ :

$$s_9 = \frac{\nu}{c_s^2} + \frac{1}{2}\Delta t \quad (4)$$

Finally, the values of density,  $\rho$ , and velocity,  $\vec{U}$ , are calculated:

$$\rho(\vec{X}, t) = \sum_{i=0}^{N-1} f_i(\vec{X}, t), \vec{U}(\vec{X}, t) = \frac{1}{\rho} \sum_{i=0}^{N-1} \vec{e}_i f_i(\vec{X}, t) \quad (5)$$

#### *Advection-diffusion equation for temperature field*

Solving advection-diffusion equation is one of the most widely used methods for simulating advection-diffusion problems. To discretize the advection-diffusion equation, a finite difference (FD) scheme is applied in this study:

$$\frac{T(\vec{X}, t + \Delta t^{\text{FD}}) - T(\vec{X}, t)}{\Delta t^{\text{FD}}} = -\vec{U} \nabla T(\vec{X}, t) + \kappa \Delta T(\vec{X}, t) \quad (6)$$

where  $T$  is the temperature and  $\Delta t^{\text{FD}}$  – the time step used in the finite-difference operation. Position  $\vec{X} = (x, y, z)$  and time  $t$  are the same as those used in LBM. Thermal diffusivity  $\kappa$  is defined:

$$\kappa = \frac{\lambda}{(\rho c_p)} \quad (7)$$

where  $\lambda$  and  $c_p$  are the heat conductivity of fluid and specific heat capacity at constant pressure, respectively. Second-order upwind interpolation scheme and second-order central interpolation scheme are adopted, respectively for the discretization of convection and diffusion terms shown in the right side of eq. (6). The value of Prandtl number  $\text{Pr} = \nu/\kappa$  is 0.71, in the assumption that the fluid is ideal air.

To ensure the stabilization of numerical simulation, the time step is confined by the LBM and the advection-diffusion equation. In LBM scheme, time step  $\Delta t$  and discretization space  $\Delta x$  are fixed. Referring to [25], the time step  $\Delta t^{\text{FD}}$  of advection-diffusion equation, which is with an advection velocity,  $\vec{U}$ , and thermal diffusivity,  $\kappa$ , has below constraint:

$$\Delta t^{\text{FD}} < \frac{(2\kappa)}{(\vec{U}\vec{U})} \quad (8)$$

#### *Smagorinsky subgrid-scale stress model*

The SGS model, introduced to LBM by Hou *et al.* [26], is applied in this work. To consider the comprehensive effect of molecular viscosity,  $\nu_0$ , and turbulent viscosity,  $\nu_t$ , molecular viscosity,  $\nu_0$ , is replaced by effective viscosity,  $\nu_{\text{eff}}$ , in this model:

$$\nu_{\text{eff}} = \nu_0 + \nu_t = \nu_0 + (C_S \Delta)^2 \sqrt{2 \sum_{\alpha, \beta} \overline{S_{\alpha\beta}} \overline{S_{\alpha\beta}}} \quad (9)$$

where  $C_S$  is Smagorinsky constant. According to our previous work [27], the value of  $C_S$  in the LBM-based simulation can be set to 0.13 to obtain accurate results,  $\Delta$  is the filter length scale and

$$\overline{S_{\alpha\beta}} = \frac{(\partial_\beta \overline{u_\alpha} + \partial_\alpha \overline{u_\beta})}{2}$$

is the filtered strain rate tensor [28]. Based on the opinion of Bardina *et al.* [28], the filter length scale used in LES is chosen as the mesh width  $\Delta = \Delta x = 1$ .

Analogously, the effect thermal diffusivity is calculated:

$$\kappa_{\text{eff}} = \kappa_0 + \kappa_t \quad (10)$$

The turbulent thermal diffusivity,  $\kappa_t$ , is related to the turbulent Prandtl number:

$$\text{Pr}_t = \frac{\nu_t}{\kappa_t} \quad (11)$$

where the value of  $\text{Pr}_t$  is set to  $\text{Pr}_t = 0.87$  [29] in this work.

## Results and discussion

### Numerical validation

The experimental results of Sinha *et al.* [30] are employed to conduct the numerical validation of the in-house HTLBM-GPU code used in present work. Table 1 summarizes the operating conditions in present work and the experiment performed by Sinha *et al.* [30], respectively. According to the comparison of numerical and experimental results, as shown in fig. 3, the predicted value of spanwise-averaged film cooling effectiveness presents a similar tendency with the experimental results [30], however, there are some deviations in the trailing edge of film cooling hole. The deviations may be due to the difference of inflow condition. In addition the differences in turbulence intensity, density ratio, there are also differences in jet-velocity distribution between this simulation and experiment of Sinha *et al.* [30]. It should be noted that the jet is ejected from a tube connected with a coolant chamber in the experiment of Sinha *et al.* [30]. While, in this simulation, the jet is just ejected from the tube. This may result in a different jet-velocity distribution. According to previous research [31, 32], the turbulence intensity, density ratio and jet-velocity distribution have a great impact on film-cooling characteristics. Therefore, the differences between experimental and numerical results are acceptable.

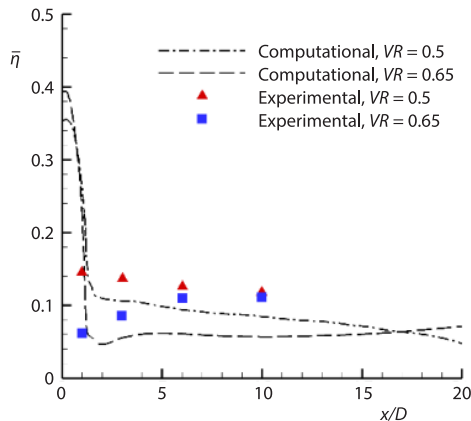


Figure 3. Comparison of numerical and experimental results

Table 1. Operating conditions of experiment and numerical simulation

Parameters	Simulation	Experiment [33]
Mainstream Reynolds number, $\text{Re}_\infty$	$1.0 \cdot 10^4$	$1.67 \cdot 10^4$
Mainstream turbulence intensity, $\text{Tu}_\infty$	0	0.2%
Velocity ratio, VR	0.5, 0.65	0.5, 0.65
Density ratio, DR	1	1.2

### Three domains of film-covering region in various cases

According to our previous work [20], the characteristics of film-covering region can be quantitatively reflected by the streamwise distribution of turbulent kinetic energy (TKE) in mid-span plane. The TKE represents the turbulence total energy. Figure 4 displays time-averaged TKE,  $k_{\text{av}}$ , in mid-span plane in the case of fig. 4(a)  $\alpha = 30^\circ$  with various BR and fig. 4(b)  $BR = 0.5$  with various inclination angles, respectively. The sym-

bols indicate the dividing points for the three domains of film-covering region. In general, the turbulence with large BR and large inclination angle is strong. Besides, the streamwise variation tendency of  $k_{av}$  changes obviously with BR and inclination angle. In the case of  $BR = 0.2$  and  $BR = 0.5$ , fig. 4(a),  $k_{av}$  rises rapidly to its maximum in rotating domain after a slow growth of shearing domain, then it drops slightly in dissipation domain. While,  $k_{av}$  with  $BR = 0.8$  shows a swift drop after reaching its maximum due to the evident dissipation. The results shown in fig. 4(b) imply that the variation tendency of  $k_{av}$  with large inclination angle is totally different. There are two peaks of  $k_{av}$  shown in rotating domain with  $\alpha = 45^\circ$  and  $\alpha = 60^\circ$ . In addition, the growth rate of  $k_{av}$  in rotating domain increases significantly as the inclination angle increases to  $\alpha = 45^\circ$  and  $\alpha = 60^\circ$ . Note that the growth ratio of  $k_{av}$  is not proportional to the growth ratio of wall-normal velocity. The maximum of  $k_{av}$  with  $\alpha = 60^\circ$  is about 4.9 times of  $\alpha = 15^\circ$ , and the wall-normal velocity in the case of  $\alpha = 60^\circ$  is about 3.5 times of  $\alpha = 15^\circ$ . However, the maximum of  $k_{av}$  with  $BR = 0.8$  is only 2.5 times of  $BR = 0.2$ , and the velocity in wall-normal direction with  $BR = 0.8$  is four times of  $BR = 0.2$ . It is implied that increasing wall-normal velocity and reducing streamwise velocity can reinforce the turbulence intensity. Therefore, the impact of inclination angle on turbulence intensity is more significant than BR.

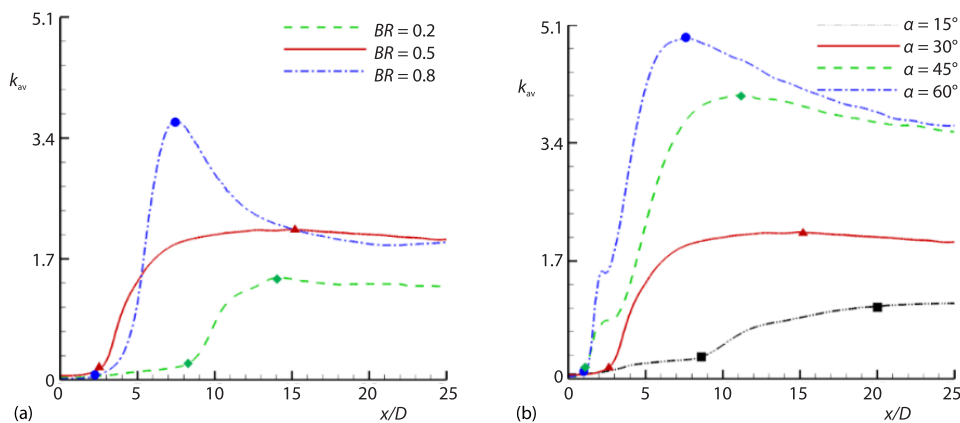
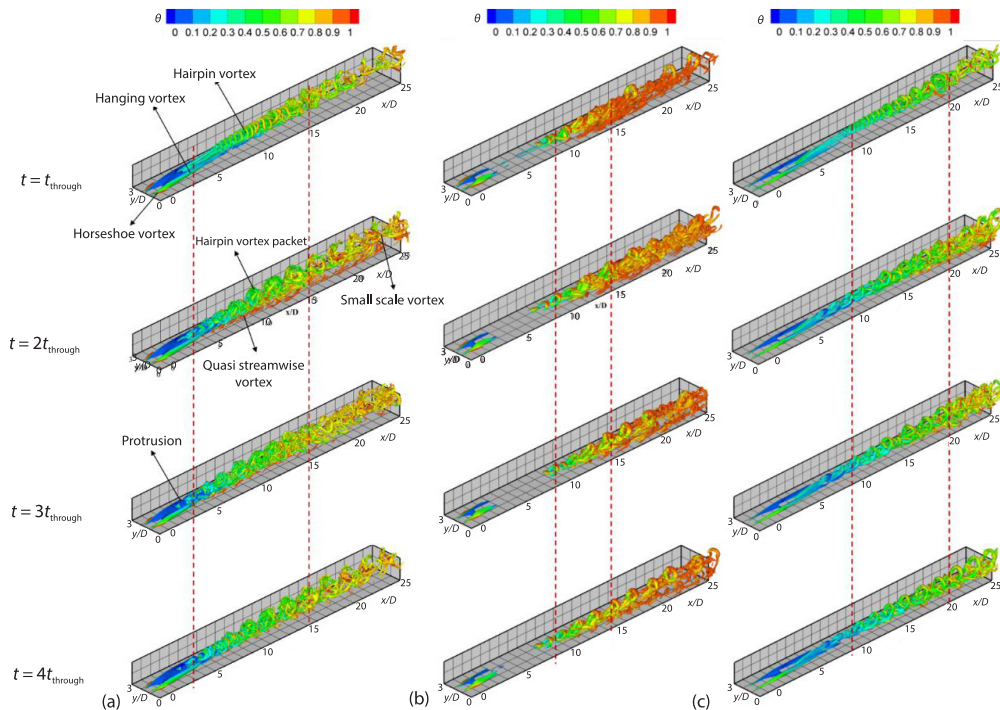


Figure 4. Time-averaged TKE,  $k_{av}$ , in mid-span plane in the case of; (a)  $\alpha = 30^\circ$  with various BR and (b)  $BR = 0.5$  with various inclination angles

### Evolution of coherent structure in three domains of film-covering region

In order to gain further insight into the evolutionary mechanism of coherent structure in each domain of film-covering region, a time sequence of coherent structure in the case of fig. 5(a)  $BR = 0.5$ ,  $\alpha = 30^\circ$ , fig. 5(b)  $BR = 0.2$ ,  $\alpha = 30^\circ$ , and fig. 5(c)  $BR = 0.5$ ,  $\alpha = 15^\circ$ , are illustrated in fig. 5. The coherent structure is presented by iso-surfaces of  $Q = 2.5$  and colored by non-dimensional temperature,  $\theta$ . The  $Q$  criterion defined in [33] is used to identify coherent structure. The initial time is  $t = t_{through}$  and the interval is  $t_{through}$ . Through-flow time  $t_{through}$  is the time required by the mean cross-flow to pass from inlet to outlet once. The dotted line indicates the partition of each domain. The spatial evolution of coherent structure in each domain varies much. In shearing domain, horseshoe vortex wrapping around the coolant jet is formed due to the blocking effect of jet. While, in rotating domain, a chain of hairpin vortices dominating the flow mixing can be observed clearly. The heads of hairpin vortices associated with the roller vortices at the interface of hot cross-flow and coolant jet entrain cross-flow into jet during

downstream propagation. Hot cross-flow exerts an upward lift on the heads of hairpin vortices, resulted from their clock-wised rotating. The legs of hairpin vortices related to counterrotating vortex pair (CVP) transport hot cross-flow beneath coolant jet, and their mutual induction also produce upward force. Therefore, hairpin vortices gradually shift away from the bottom wall in evolution. The stretching distortion and breakup of hairpin vortices occur as they propagate downstream. In dissipation domain, the hairpin vortices breakup into disordered small-scale vortices.



**Figure 5. A time sequence of instantaneous coherent structure downstream of film cooling hole in the case of; (a)  $BR = 0.5$ ,  $\alpha = 30^\circ$  and (b)  $BR = 0.2$ ,  $\alpha = 30^\circ$ , and (c)  $BR = 0.5$ ,  $\alpha = 15^\circ$**

Besides, the structure form of vortices in each domain changes over time. As shown in fig. 5(a), only a pair of hanging vortices locating at the both lateral sides of film cooling hole in shearing domain at  $t = t_{\text{through}}$ , which give a path downstream to coolant jet and provide the circulation necessary to create CVP [34]. Then, an obvious protrusion just at the downstream of film cooling hole can be observed at  $t = 3t_{\text{through}}$  and  $t = 4t_{\text{through}}$ . The protrusion is related to generation of hairpin vortex happening in rotating domain. As for hairpin vortices, at the initial time,  $t = t_{\text{through}}$ , they appear at the location of  $x/D = 7.0$ . Both the size and strength of hairpin vortices increase while propagating downstream. The behaviors of hairpin vortices promote hot cross-flow mixing with coolant jet, leading to the intensified heat transfer nearby the bottom wall, which is adverse to the protection of the bottom wall against direct contact with hot cross-flow. Since from the following time, hairpin vortices appear at the beginning of rotating domain,  $x/D = 7.0$ , and change into complex hairpin packets quickly. Except for hairpin packets, rod-like quasi-streamwise vortices with high temperature lie on the bottom wall. The unsteady quasi-streamwise vortices can be observed obviously at  $t = 2t_{\text{through}}$  and transport hot cross-flow beneath coolant jet, making the flow pattern more complex and

convective heat transfer stronger. In dissipation domain, small-scale vortices with high temperature distribute disorderly and their distribution are more and more disorganized as they propagate to the far field region.

The results shown in figs. 5(b) and 5(c) illustrate that the evolution process of coherent structure is different by changing BR and inclination angle. Compared to large-blowing-ratio case, the size of coherent structure in small BR changes significantly. The width of coherent structure with  $BR = 0.2$ ,  $\alpha = 30^\circ$  is larger than that of  $BR = 0.5$ ,  $\alpha = 30^\circ$ , while the height of coherent structure in small-blowing-ratio case is smaller, suggesting that the coolant film has a good attachment to the bottom wall in the case of small BR. Besides, the integral morphology of coherent structure has evident change as inclination angle decrease from  $\alpha = 30^\circ$  to  $\alpha = 15^\circ$ . In the case of  $BR = 0.5$ ,  $\alpha = 15^\circ$ , the hairpin vortices maintain a relatively intact shape and they start to change into hairpin packets at the latter half of rotating domain. Moreover, there are very few quasi-streamwise vortices shown in the case of  $BR = 0.5$ ,  $\alpha = 15^\circ$  and the small-scale vortices arising in dissipation domain are in more orderly arrangement than that of  $BR = 0.5$ ,  $\alpha = 30^\circ$ .

### Analysis of time-averaged temperature field

Figure 6 shows the contours of time-averaged film cooling effectiveness,  $\eta$ , on the bottom wall in the case of  $\alpha = 30^\circ$  with various BR of fig. 6(a)  $BR = 0.2$ , fig. 6(b)  $BR = 0.5$ , and fig. 6(c)  $BR = 0.8$ . In general, the coverage of coolant film decreases with the increasing BR. The coolant jet with large BR shows the tendency to detach from the bottom wall, leading to small coolant-film coverage.

The contours of time-averaged film cooling effectiveness,  $\eta$ , on the bottom wall in the case of  $BR = 0.5$  with various inclination angles of fig. 7(a)  $\alpha = 15^\circ$ , fig. 7(b)  $\alpha = 30^\circ$ , fig. 7(c)  $\alpha = 45^\circ$ , and fig. 7(d)  $\alpha = 60^\circ$  are demonstrated in fig. 7. It can be observed that the coverage of stable coolant film reduces with the increasing of inclination angle. However, the coolant-film coverage in the case of  $BR = 0.5$  with various inclination angles is smaller than that of  $BR = 0.2$ ,  $\alpha = 30^\circ$ , fig. 6(a). Along with the BR reducing, the velocity of coolant jet decreases both in the streamwise and wall-normal direction. While, only the wall-normal velocity of coolant jet decreases with reducing inclination angle. It seems that the small streamwise velocity contributes significant benefit to the good attachment of coolant film to the bottom wall, which results in large coverage of coolant film.

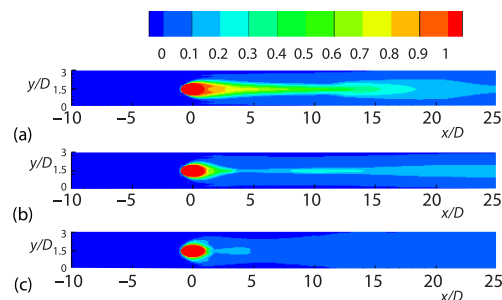


Figure 6. The contours of time-averaged film cooling effectiveness,  $\eta$ , on the bottom wall in the case of  $\alpha = 30^\circ$  with various blowing ratios of; (a)  $BR = 0.2$ , (b)  $BR = 0.5$ , and (c)  $BR = 0.8$

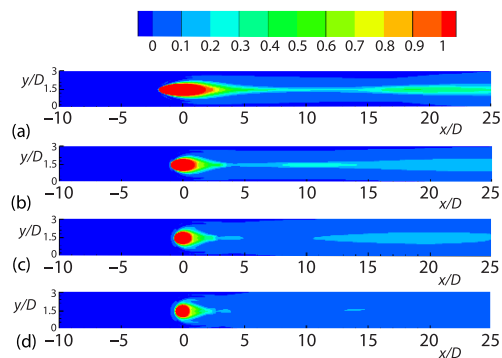
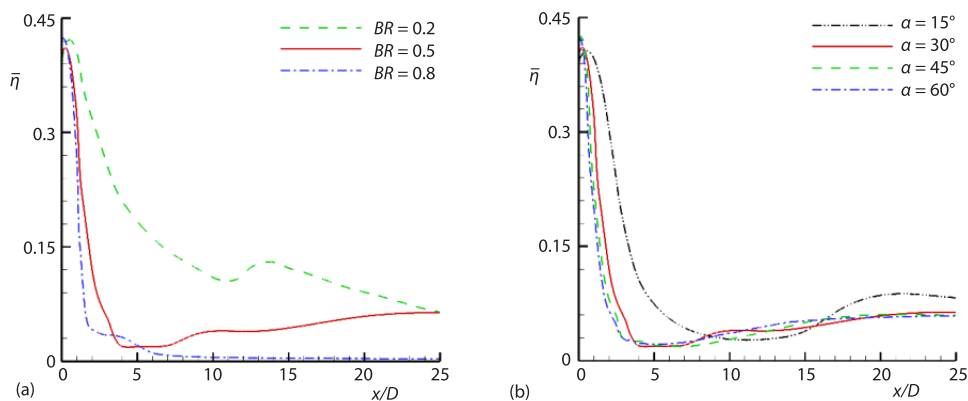


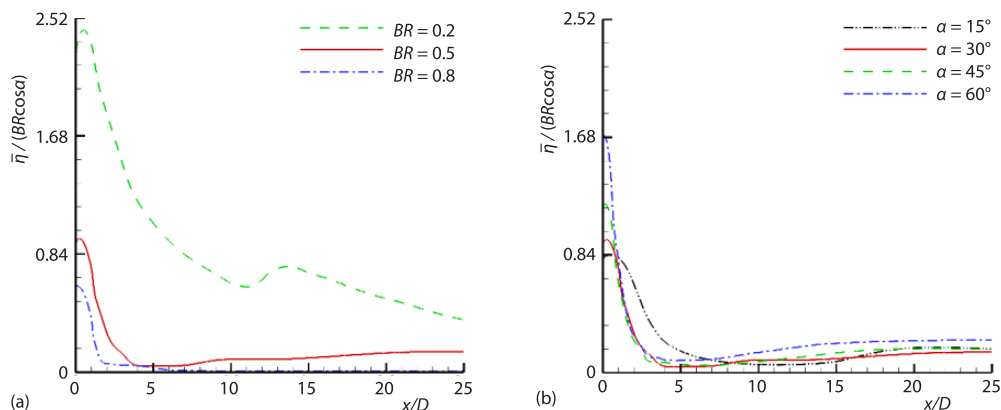
Figure 7. The contours of time-averaged film cooling effectiveness,  $\eta$ , on the bottom wall in the case of  $BR = 0.5$  with various inclination angles of; (a)  $\alpha = 15^\circ$ , (b)  $\alpha = 30^\circ$ , (c)  $\alpha = 45^\circ$ , and (d)  $\alpha = 60^\circ$

Figure 8 displays spanwise-averaged film cooling effectiveness,  $\bar{\eta}$ , in the case of fig. 8(a)  $\alpha = 30^\circ$  with various BR and fig. 8(b)  $BR = 0.5$  with various inclination angles. Generally,  $\bar{\eta}$  decreases with the increasing of BR or inclination angle. It is noted that the changing trends of  $\bar{\eta}$  with various BR are different. However, it changes little in the case of various inclination angles. In particular, the curve of  $\bar{\eta}$  in the case of  $BR = 0.5$ ,  $\alpha = 45^\circ$  almost overlap with that of  $BR = 0.5$ ,  $\alpha = 60^\circ$ . The penetration of jet into cross-flow is the key factor of distribution of  $\bar{\eta}$ . It may be because that the jet penetration with  $BR = 0.5$ ,  $\alpha = 45^\circ$  is too strong to continue to grow by increasing inclination angle from  $\alpha = 45^\circ$  to  $\alpha = 60^\circ$ . This further clarify that BR is a factor having a significant influence on film-cooling performance.



**Figure 8.** Spanwise-averaged film cooling effectiveness,  $\bar{\eta}$ , in the case of; (a)  $\alpha = 30^\circ$  with various BR and (b)  $BR = 0.5$  with various inclination angles

Figure 9 demonstrates spanwise-averaged film cooling effectiveness per streamwise coolant discharge  $\bar{\eta}/BR\cos\alpha$  in the case of fig. 9(a)  $\alpha = 30^\circ$  with various BR and fig. 9(b)  $BR = 0.5$  with various inclination angles to study the film-cooling performance of per unit streamwise coolant discharge in different cases. The  $\bar{\eta}/BR\cos\alpha$  decreases along with increasing BR, however, it increases with the increasing of inclination angle. This phenomenon suggests that the cooling efficiency of per streamwise coolant-jet discharge is also closely linked to streamwise velocity of coolant jet. Reducing jet velocity in streamwise direction can improve



**Figure 9.** Spanwise-averaged film cooling effectiveness per streamwise coolant discharge  $\bar{\eta}/BR\cos\alpha$  in the case of; (a)  $\alpha = 30^\circ$  with various BR and (b)  $BR = 0.5$  with various inclination angles

its cooling efficiency under the certain conditions. Moreover, the values of  $\bar{\eta}/BR\cos\alpha$  with various BR, fig. 9(a), show a higher rate of change than those with various inclination angles, fig. 9(b). It further indicate that the effect of BR on film-cooling performance is more significant than inclination angle.

## Conclusions

The present study employs HTLBM and multi-GPU to numerically investigate the evolutionary mechanism of coherent structure in film-cooling process. Besides, the influencing mechanism of BR and inclination angle on unsteady behaviors of flow structures and film-cooling performance are studied. From the simulation results, it can be concluded as follows.

- There are various vortices generating in film-covering region. Among them, hairpin vortex, hairpin packet and quasi-streamwise vortex appearing in rotating domain play a significant role in the mixing mechanism of film cooling. The prominent ejection, sweep and vortex rotation made by these vortices result in the significant convective heat transfer. Besides, the width and height of coherent structure change much with various BR, however, the integral form varies obviously with inclination angle.
- Inclination angle of coolant jet has a significant impact on turbulence fluctuation intensity. The large wall-normal jet velocity and small streamwise jet velocity in the case of large inclination angle lead to significant penetration of coolant jet into hot cross-flow and intense shearing between coolant jet and cross-flow. All of these enhance flow mixing and turbulence fluctuation.
- The influence of BR on the attachment of coolant film and film-cooling performance is more remarkable than inclination angle. The attachment of coolant film, film cooling effectiveness and cooling efficiency of per streamwise coolant-jet discharge can be improved significantly by reducing BR. The slow streamwise jet velocity in the case of small BR make more time for coolant jet to attach to the bottom wall.

## Acknowledgment

The work was supported by Basic Research Program of Jiangsu Province [Grant No. BK20200182], the Fellowship of China Postdoctoral Science Foundation [Grant No. 2020M671314], the Fundamental Research Funds for the Central Universities of China [Grant No. B210202128], Open Projects of State Key Laboratory for Strength and Vibration of Mechanical Structures in Xi'an Jiaotong University [Grant No. SV-2020-KF-04], Open Fund of Key Laboratory of Icing and Anti/De-icing [Grant No. IADL20190302] and the Research on Smart Operation Control Technologies for Offshore Wind Farms (Grant No. 2019YFE0104800).

## Nomenclature

$BR$ – blowing ratio, $(= \rho_j u_j / \rho_x u_x)$ , [-]	$L$ – domain length, [m]
$C_s$ – Smagorinsky constant, [-]	$l$ – hole length, [m]
$c_p$ – specific heat capacity at constant pressure, [Jkg <sup>-1</sup> K <sup>-1</sup> ]	$[M]$ – transfer matrix, [-]
$c_s$ – speed of sound, [ms <sup>-1</sup> ]	$\bar{m}$ – velocity moments, [m <sup>2</sup> s <sup>-1</sup> ]
$D$ – diameter of cooling hole, [m]	$\bar{m}^{eq}$ – equilibria of velocity moments, [m <sup>2</sup> s <sup>-1</sup> ]
$\bar{e}_i$ – discrete velocity of particle of $i$ -direction, [ms <sup>-1</sup> ]	$Pr$ – Prandtl number, $(= \nu/\kappa)$ , [-]
$f_i$ – particle density distribution function of $i$ -direction, [-]	$Q$ – invariants of the velocity gradient used to depict turbulence coherent structure, [ms <sup>-2</sup> ]
$k$ – turbulent kinetic energy, [J]	$Re$ – Reynolds number, $(= \rho u_x D / \nu)$ , [-]
$k_{av}$ – time-averaged turbulent kinetic energy, [J]	$[S]$ – relaxation matrix, [-]
	$\bar{S}_{\alpha\beta}$ – filtered strain rate tensor, [-]
	$s_i$ – relaxation rate of $i$ -direction, [-]

$T$  – temperature, [K]  
 $t$  – time, [s]  
 $\Delta t$  – time step of lattice Boltzmann method, [s]  
 $\Delta t^{\text{FD}}$  – time step used in the finite difference operation, [s]  
 $\vec{U}$  – velocity, [ $\text{ms}^{-1}$ ]  
 $\vec{X}$  – position with Cartesian co-ordinate system, [–]  
 $x$  – Cartesian co-ordinate system in streamwise direction, [–]  
 $\Delta x$  – lattice spacing of lattice Boltzmann method, [m]  
 $y$  – Cartesian co-ordinate system in spanwise direction, [–]  
 $z$  – Cartesian co-ordinate system in wall-normal direction, [–]

#### Greek symbols

$\alpha$  – inclination angle of coolant jet, [ $^{\circ}$ ]  
 $\eta$  – film cooling effectiveness, ( $= T_{\infty} - T_{\text{aw}}/T_{\infty} - T_j$ ), [–]  
 $\bar{\eta}$  – spanwise-averaged film cooling effectiveness, [–]  
 $\theta$  – non-dimensional temperature, ( $= T_{\text{aw}} - T_j/T_{\infty} - T_j$ ), [–]  
 $\Delta$  – filter length scale, [m]

$\kappa$  – thermal diffusivity, [ $\text{m}^2\text{s}^{-1}$ ]  
 $\lambda$  – heat conductance of fluid, [ $\text{Wm}^{-1}\text{K}^{-1}$ ]  
 $\nu$  – kinematic shear viscosity, [ $\text{m}^2\text{s}^{-1}$ ]  
 $\rho$  – density, [ $\text{kgm}^{-3}$ ]

#### Subscripts

aw – adiabatic wall  
 eff – effective  
 j – coolant jet flow  
 t – turbulent  
 through – through-flow  
 $\infty$  – hot crossflow  
 0 – molecular

#### Acronyms

CVP – counterrotating vortex pair  
 DR – density ratio, ( $=\rho_j/\rho_{\infty}$ )  
 FD – finite difference  
 GPU – graphic processing unit  
 HTLBM – hybrid thermal lattice Boltzmann method  
 LBM – lattice Boltzmann method  
 LES – large eddy simulation  
 PR – density  
 SGS – Smagorinsky subgrid-scale stress  
 TKE – turbulent kinetic energy  
 VR – velocity ratio, ( $=V_j/V_{\infty}$ )

#### References

- [1] Bogard, D. G., Thole, K. A., Gas Turbine Film Cooling, *Journal of Propulsion and Power*, 22 (2006), 2, pp. 249-270
- [2] Han, J. C., et al., *Gas Turbine Heat Transfer and Cooling Technology*, CRC Press, Boca Raton, Fla., USA, 2000
- [3] Acharya, S., Film Cooling Simulation and Control, *Heat Transfer Research*, 41 (2010), 6, pp. 601-626
- [4] Li, G. Q., Deng, H. W., Experimental Investigation on Film Cooling Performance of Pressure Side in Annular Cascades, *Journal of Thermal Science*, 20 (2011) 2, pp. 119-126
- [5] Vijayakumar, V., et al., Computational and Experimental Study on Supersonic Film Cooling for Liquid Rocket Nozzle Applications, *Thermal Science*, 19 (2015), 1, pp. 49-58
- [6] Xie, Y. H., et al., Numerical Study on Film Cooling and Convective Heat Transfer Characteristics in the Cutback Region of Turbine Blade Trailing Edge, *Thermal Science*, 20 (2016), 3, pp. S643-S649
- [7] Wang, J., et al., Effect of Spherical Blockage Configurations on Film Cooling, *Thermal Science*, 28 (2018), 5, pp. 1933-1942
- [8] Ravi, D., Parammasivam, K. M., Enhance Film Cooling Effectiveness in a Gas Turbine End-Wall with a Passive Semicylindrical Trench, *Thermal Science*, 23 (2019), 3, pp. 2013-2023
- [9] Lakehal, D., et al., Computation of Film Cooling of Flat Plate by Lateral Injection from a Row of Holes, *International Journal of Heat and Fluid-Flow*, 19 (1998), 5, pp. 418-430
- [10] Theodoridis, G. S., et al., The 3-D Calculations of the Flow Field Around a Turbine Blade with Film Cooling Injection Near the Leading Edge, *Flow, Turbulence and Combustion*, 66 (2001), 1, pp. 57-83
- [11] Dyson, T. E., et al., Evaluation of CFD Simulations of Film Cooling Performance on a Turbine Vane Including Conjugate Heat Transfer Effects, *International Journal of Heat and Fluid-Flow*, 50 (2014), Dec., pp. 279-286
- [12] Galeazzo, F. C. C., et al., Computational Modelling of Turbulent Mixing in a Jet in Crossflow, *International Journal of Heat and Fluid-Flow*, 41 (2013), June, pp. 55-65
- [13] Renze, P., et al., Large-Eddy Simulation of Film Cooling Flows at Density Gradients, *International Journal of Heat and Fluid-Flow*, 29 (2008), Feb., pp. 18-34
- [14] Shangguan, Y. Q., et al., Large-Scaled Simulation on the Coherent Vortex Evolution of a Jet in a Cross-Flow Based on Lattice Boltzmann Method, *Thermal Science*, 19 (2015), 3, pp. 977-988

- [15] Qenawy, M., et al., Flow Structures and Unsteady Behaviors of Film Cooling from Discrete Holes Fed by Internal Crossflow, *Journal of Turbomachinery*, 142 (2020), 4, 041007
- [16] Andrew, D., et al., Evaluation of Massively-Parallel Spectral Element Algorithm for LES of Film-Cooling, *Proceedings*, ASME Turbo Expo 2013: Turbine Technical Conference and Exposition, San Antonio, Tex., USA, 2013, Paper No. GT2013-94281
- [17] Fatahalian, K., et al., Brook for GPU: Stream Computing on Graphics Hardware, *ACM Transactions on Graphics*, 23 (2004), 3, pp. 777-786
- [18] Chen, S. Y., Doolen, G. D., Lattice Boltzmann Method for Fluid-flows, *Annual Review of Fluid Mechanics*, 30 (1998), 1, pp. 329-364
- [19] Wang, X., Aoki, T., Multi-GPU Performance of Incompressible Flow Computation by Lattice Boltzmann Method on GPU Cluster, *Parallel Computing*, 37 (2001), 9, pp. 521-535
- [20] Shangguan, Y. Q., et al., Investigation on the Mixing Mechanism of Single-Jet Film Cooling with Various Blowing Ratios Based on Hybrid Thermal Lattice Boltzmann Method, *International Journal of Heat and Mass Transfer*, 97 (2016), June, pp. 880-890
- [21] Shangguan, Y. Q., et al., The LBM Study on Unsteady Flow and Heat Transfer Behaviors of Double-Row Film Cooling with Various Row Spacings, *International Journal of Heat and Mass Transfer*, 138 (2019), Aug., pp. 1251-1263
- [22] Kruger, T., et al., *The Lattice Boltzmann Method: Principle and Practice*, Springer, Berlin, Germany, 2016
- [23] Lallemand, P., Luo, L. S., Theory of the Lattice Boltzmann Method: Acoustic and Thermal Properties in Two and Three Dimensions, *Physical Review E*, 68 (2003), 3, pp. 999-1005
- [24] d'Humieres, D., et al., Multiple-Relaxation-Time Lattice Boltzmann Models in Three Dimensions, *Philosophical Transactions of the Royal Society A*, 360 (2002), 1972, pp. 437-451
- [25] Hirsch, G., *Numerical Computation of Internal and External Flows*, John Wiley, New Jersey, N. Y., USA, 1988
- [26] Hou, S., et al., A Lattice Boltzmann Subgrid Model for High Reynolds Number Flows, *Fields Institute Communications*, 6 (1994), 13, pp. 151-168
- [27] Wang, X., et al., Direct Numerical Simulation and Large Eddy Simulation on a Turbulent Wall-Bounded Flow Using Lattice Boltzmann Method and Multiple GPU, *Mathematical Problems in Engineering*, 2014 (2014), 742432
- [28] Bardina, J., et al., Effect of Rotation on Isotropic Turbulence-Computation and Modelling, *Journal of Fluid Mechanics*, 154 (1985), May, pp. 321-336
- [29] Schlichting, H., Gersten, K., *Boundary-Layer Theory*, Springer, Berlin, Germany, 2000
- [30] Sinha, A. K., et al., Film-Cooling Effectiveness Downstream of a Single Row of Holes with Variable Density Ratio, *Journal of Turbomachinery*, 133 (1991), 4, pp. 442-449
- [31] Stratton, Z. T., Shih T. I. P., Effects of Density and Blowing Ratios on the Turbulent Structure and Effectiveness of Film Cooling, *Journal of Turbomachinery*, 140 (2018), 10, 101007
- [32] An, B. T., et al., Effects of Mainstream Turbulence Intensity and Coolant-to-Mainstream Density Ratio on Film Cooling Effectiveness of Multirow Diffusion Slot Holes, *Journal of Heat Transfer*, 141 (2019), 12, 122001
- [33] Hunt, J. R., et al., Eddies, Streams, and Convergence Zones in Turbulent Flows, Report No. CTR-S88, Stanford University, Ames, Ca., USA, 1998
- [34] Walters, D. K., Leylek, J. H., A Detailed Analysis of Film-Cooling Physics: Part I-Streamwise Injection with Cylindrical Holes, *Journal of Turbomachinery*, 122 (2000), 1, pp. 102-112